Synthetic Biology and Engineering

SciEPublish

Article

Investigating the Impact of Measurement Variance on Parameterization: A Case Study of Synthetic Gene Circuits

Thales R. Spartalis [1], Kaylee Meng [2], Wan Tang [3,*] and Xun Tang [1,*]

[1] Cain Department of Chemical Engineering, Louisiana State University, Baton Rouge, LA 70803, USA; tspart1@lsu.edu (T.R.S.)

[2] Baton Rouge Magnet High School, Baton Rouge, LA 70806, USA; km1009994@ebrstudents.org (K.M.)

[3] Celia Scott Weatherhead School of Public Health & Tropical Medicine, Tulane University, New Orleans, LA 70112, USA

* Corresponding author. E-mail: wtang1@tulane.edu (W.T.); xuntang@lsu.edu (X.T.)

Received: 21 September 2026; Revised: 23 October 2026; Accepted: 2 November 2026; Available online: 16 November 2026

ABSTRACT: Ordinary differential equation (ODE) models are widely used to characterize synthetic gene circuits, but estimating model parameters from fluorescence-based gene expression data can be challenging. This study examines whether measurement variance should be incorporated into objective functions and whether objective function formulation can benefit parameter identifiability. We fitted mechanistic models of a toehold-switch AND gate and a CRISPR interference (CRISPRi) regulator to cell-free experimental measurements using unweighted least squares, inverse-variance weighting, and relative-variance weighting under raw and noise-augmented data. The three objectives produced similar trajectory fits, with relative-variance weighting showing modest robustness under higher noise, while inverse-variance weighting was less consistent. Profile-likelihood analysis showed that residual weighting did not resolve practical non-identifiability. These findings were then cross validated using an independent STAR circuit. Consistently, objective function choice had limited impact on fitting or parameter identifiability. To further examine parameter identifiability, we reduced the original eight-parameter STAR model to a three-state, four-parameter model and found that reduced model complexity can lead to local parameter identifiability, at the cost of reduced approximation accuracy to the time-course measurements. While this study focused on three representative gene circuits, we anticipate future studies across a broader range of circuit architectures to establish more general conclusions regarding the impact of measurement variance on model parameterization.

Keywords: Gene circuits; Model parameterization; Measurement variance; Profile likelihood; Structural identifiability; Synthetic biology; Cell-free systems

1. Introduction

Mathematical modeling is an important tool in synthetic biology, supporting the interpretation of biological networks, the design of synthetic regulatory circuits, and the development of diagnostic and therapeutic applications [1–4]. Synthetic gene circuits are assembled from biomolecular components, including DNA, RNA, and proteins, to produce defined functions through designed molecular interactions.

© 2026 The authors. This is an open access article under the Creative Commons Attribution 4.0 International License (https://creativecommons.org/licenses/by/4.0/).

Characterizing the properties of a new circuit before practical implementation is important for confirming that a design behaves as intended. While cell-free transcription and translation (TXTL) systems provide controlled environments for circuit characterization and support high-throughput measurements, mathematical models can complement these experiments by using gene expression data to infer interactions, describe system dynamics, and examine the mechanisms that shape circuit behavior [4–6].

The dynamics of a synthetic gene circuit can be described with parametric models, such as partial or ordinary differential equations (ODEs), and with non-parametric models, such as Markov state models and artificial neural networks [5,7–14]. Deterministic ODE-based models are among the simplest and most popular models for gene circuit dynamics simulation. These models represent the time evolution of molecular species from known or hypothesized reaction mechanisms [10–12], and their accuracy depends on the model structure, the correctness of the assumed reactions, and the values of kinetic parameters such as transcription, translation, degradation, and binding rates [15–19]. Estimating these kinetic parameters, a process referred to here as model parameterization, is a long-standing challenge because ODE models can be stiff, contain many coupled parameters, and are often informed by limited experimental measurements [20–23].

Parameterization is typically achieved by minimizing a cost function that quantifies the discrepancy between the simulated and the measured outputs. The formulation of the objective can change the fitted parameters, because it encodes an assumption about how model predictions relate to noisy observations [24–26]. While this objective function can take various forms [21,27], the sum of pairwise squared errors is one of the most common objectives because of its simplicity and ease of interpretation. Inverse-variance-weighted squared error has also been used to account for measurement precision, so that the residual at each time point is weighted by the estimated measurement variance at that instant. Weighted objectives have been studied in several modeling and calibration settings [28–30], but their use in synthetic gene circuit parameterization remains comparatively underexamined, even though measurement variance is especially relevant for fluorescence time courses, as replicate spread can change over time. This measurement variance could potentially matter more when fluorescence is the only measured output to parameterize the model, as it captures only part of the molecular state described by the model. Under these conditions, the objective function weighting can interact with parameter correlations, limited data informativeness, and practical non-identifiability, so that a good trajectory fit does not by itself infer the unique or precise identifiability of individual kinetic parameters [21–23,30,31].

In this study, we investigate whether incorporating experimental measurement variance into commonly used objective functions benefits gene circuit model parameterization in terms of output time-course dynamics approximation and model parameter identifiability. Specifically, we consider three RNA-based synthetic gene circuits: a toehold-switch AND gate, a CRISPR interference regulator, and a small transcription-activating RNA system, referred to as STAR [32–34]. We compare three formulations of the objective function: a baseline that leaves all residuals unweighted, a formulation that weights each residual by the inverse of the measured variance, and a formulation that weights each residual by the variance relative to the signal. For brevity, we refer to these objective functions as the No Variance, Variance, and Relative Variance objectives, respectively. We found that the unweighted objective function can yield satisfactory fitting results across different levels of measurement variance, whereas weighting directly with measurement variance rather than relative variance could potentially undermine fitting performance. Furthermore, a good fit to the output trajectory does not necessarily indicate parameter identifiability, which could potentially be improved by reducing model complexity, although at the cost of increased fitting error. These findings further suggest that weighting the objective function using relative measurement variance could potentially benefit scenarios where measurement variance is significant, and that a tradeoff exists between model fitting accuracy and parameter identifiability.

2. Methods

2.1. Study Design

We first focused on a toehold-switch AND gate and a CRISPRi regulator to evaluate the impact of measurement variance on trajectory-fitting accuracy and model parameter identifiability, using raw cell-free experimental measurements. We then extended the analysis to a STAR system for validation, using both a controlled set of synthetic data and raw cell-free experimental measurements. By varying the complexity of the STAR model, we further investigated the impact of measurement variance on fitting accuracy and parameter identifiability, taking advantage of the simpler mechanistic description this system provides, which enabled structural-identifiability analysis with GenSSI 2.0 [35]. In all cases, three objective functions were compared (No Variance, Variance, and Relative Variance; Section 2.4), GFP fluorescence was the only measured output, and replicate measurements at each sampled time point were summarized by their mean and sample variance before parameterization. The three circuits are shown in Figure 1.

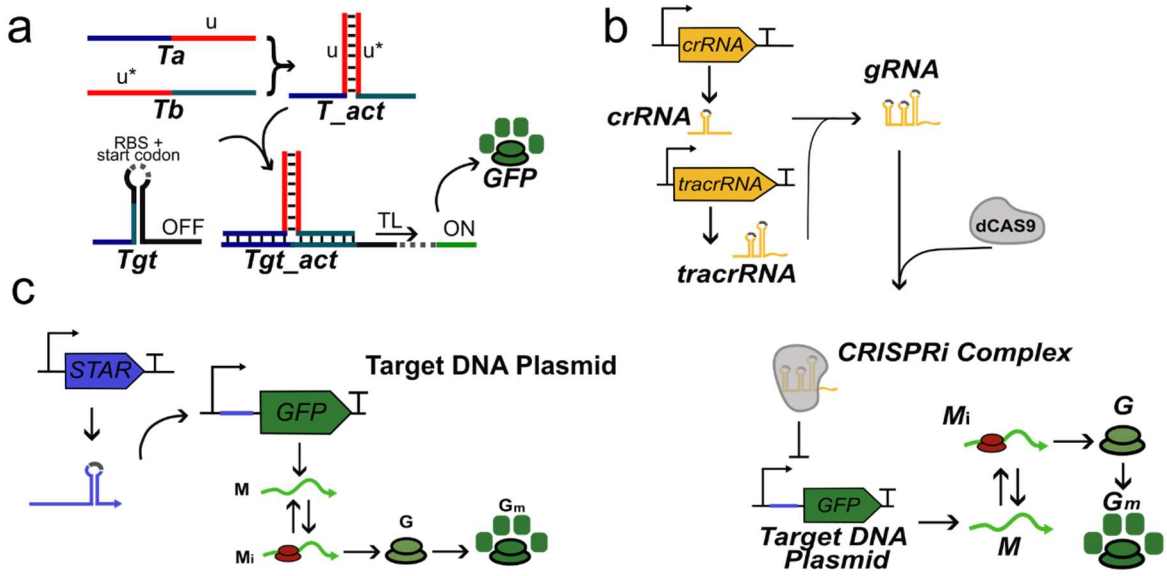


Figure 1. Overview of the three RNA-based synthetic gene circuits studied. (**a**) Toehold-switch AND gate: two trigger RNAs (*Ta* and *Tb*) hybridize through a shared complementary sequence (u,u*) to form the active trigger complex, which opens the target RNA hairpin and enables translation of GFP; in the absence of either trigger, translation is not activated. (**b**) CRISPR interference (CRISPRi) regulator: separately transcribed crRNA and tracrRNA hybridize to form the guide RNA, which binds dCas9 to form a repression complex that binds the target promoter and blocks transcription of the GFP cassette. (**c**) STAR circuit: the STAR RNA relieves the transcriptional block on the target template, permitting downstream transcription and GFP expression. GFP fluorescence is the measured output in all three circuits.

2.2. Toehold-Switch AND Gate and CRISPRi Models

The toehold-switch AND gate contains two trigger RNAs, *Ta* and *Tb*, which hybridize through a shared complementary sequence to form the active trigger complex *Tact*. The individual triggers and the complex open the target RNA and enable GFP translation; without either trigger, translation is not activated, and the gene is not expressed. The model represents the activation mechanism used in toehold-switch and ribocomputing systems [32,36,37]. The AND-gate measurements were collected from TXTL experiments following an established extract and template preparation protocol [38]. Reactions used an *Escherichia coli* BL21(DE3) Star cell extract supplemented with the standard energy, nucleotide, amino acid, and salt components required for transcription and translation, following an established protocol [37]. DNA templates were amplified by PCR and purified with a PCR purification kit. Reactions were incubated at 30 °C, and GFP fluorescence was recorded every 10 min on a BioTek Synergy plate reader–Agilent

Technologies, Inc., Santa Clara, CA, USA. The detailed model of the AND gate circuit is given as in Equation (1), where C_{Ta}, C_{Tb}, and C_{Tgt} represent the template concentrations for the two trigger RNAs and the target RNA, respectively. The parameter α is the transcription rate used to generate each RNA species from its corresponding template. δ_{Ta}, δ_{Tb}, δ_{Tgt}, $\delta_{Tgt_{act}}$, and δ_G denote the degradation or loss rates of the corresponding trigger RNA, target RNA, activated target RNA, and GFP species. The parameter β_T is the RNA hybridization rate that forms T_{act} from T_a and T_b, whereas ν is the dissociation rate of T_{act}. The terms β_{basal}, β_{Ta}, β_{Tb}, and β_{Tact} describe basal and trigger dependent opening of the target RNA hairpin. K_i and K_e describe the effective forward and reverse rates associated with the translation intermediate M_i, K_{TL} is the GFP translation rate, K_a, K_b, and K_{act} are the half maximal constants in the Hill activation functions, and n is the Hill coefficient.

$$\frac{dT_a}{dt} = \alpha \cdot C_{Ta} + \nu \cdot [T_{act}] - \beta_T \cdot [T_b] \cdot [T_a] - \delta_{Ta} \cdot [T_a]$$

$$\frac{dT_b}{dt} = \alpha \cdot C_{Tb} + \nu \cdot [T_{act}] - \beta_T \cdot [T_b] \cdot [T_a] - \delta_{Tb} \cdot [T_b]$$

$$\frac{dT_{act}}{dt} = \beta_T \cdot [T_b] \cdot [T_a] - \nu \cdot [T_{act}]$$

$$\frac{dTgt}{dt} = \alpha \cdot C_{Tgt} - \delta_{Tgt} \cdot [Tgt] - \beta_H$$

$$\frac{dTgt_{act}}{dt} = \beta_H - \delta_{Tgt_{act}} \cdot [Tgt_{act}] - \mathrm{K}_i \cdot [Tgt_{act}] + \mathrm{K}_e \cdot [M_i]$$

$$\frac{dM_i}{dt} = \mathrm{K}_i \cdot [Tgt_{act}] - \mathrm{K}_e \cdot [M_i]$$

$$\frac{dG}{dt} = \mathrm{K}_{TL} \cdot [M_i] - \delta_G \cdot [G]$$

$$\beta_H = [Tgt] \cdot \left(H_{T_a} + H_{T_b} + H_{T_{act}} + \beta_{basal}\right)$$

$$H_{T_a} = \beta_{Ta} \cdot \frac{[T_a]^n}{[T_a]^n + {K_a}^n}$$

$$H_{T_b} = \beta_{Tb} \cdot \frac{[T_b]^n}{[T_b]^n + {K_b}^n}$$

$$H_{T_{act}} = \beta_{Tact} \cdot \frac{[T_{act}]^n}{[T_{act}]^n + {K_{act}}^n} \quad (1)$$

The CRISPRi circuit uses separate crRNA and tracrRNA templates. The transcribed RNAs hybridize to form the guide RNA, which binds dCas9 to form a repression complex that binds the target promoter and blocks transcription. The model includes guide-RNA production, dCas9 complex formation, promoter repression, mRNA production, translation, and GFP maturation [33,34,39]. The CRISPRi measurements were taken from a previous cell-free study [39] and consist of GFP time courses at different plasmid concentrations. The CRISPRi measurements consist of GFP fluorescence time courses collected under three conditions, defined by the concentration of the CRISPRi components forming the repression complex: 0 nM (no-interference control), 0.10 nM, and 0.25 nM. Increasing concentration increases the degree of transcriptional repression, and the three resulting time courses were used for model calibration. The detailed mechanistic model is given in Equation (2), same as in ref. [39] P_y^- is the concentration of target promoters occupied by the repression complex, and P_y is the free target promoter concentration. P_{cr}, P_{tr}, and P_y^{tot} are

the fixed template concentrations for $crRNA$, $tracRNA$, and the total target promoter. The parameters α_{cr}, α_{tr}, and α_m are the transcription rates of $crRNA$, $tracRNA$, and target mRNA, respectively. The parameters δ_{cr}, δ_{tr}, δ_g, and δ_m denote the degradation or loss rates of $crRNA$, $tracRNA$, guide RNA, and target mRNA. γ_1 and γ_2 describe the $crRNA - tracRNA$ hybridization and $gRNA - dCAS9$ complex formation rates, respectively. The parameter ω is the promoter binding rate for the repression complex. K_i and K_e describe the effective forward and reverse rates associated with the translation intermediate M_i, and α_{gm} is the GFP maturation rate that converts G to G_m.

$$\frac{dcrRNA}{dt} = \alpha_{cr} \cdot P_{cr} - \delta_{cr} \cdot [crRNA] - \gamma_1 \cdot [crRNA] \cdot [tracrRNA]$$

$$\frac{dtracRNA}{dt} = \alpha_{tr} \cdot P_{tr} - \delta_{tr} \cdot [tracrRNA] - \gamma_1 \cdot [crRNA] \cdot [tracRNA]$$

$$\frac{dgRNA}{dt} = \gamma_1 \cdot [crRNA] \cdot [tracRNA] - \gamma_2 \cdot [gRNA] \cdot [dCAS9] - \delta_g \cdot [gRNA]$$

$$\frac{ddCAS9}{dt} = -\gamma_2 \cdot [gRNA] \cdot [dCAS9]$$

$$\frac{dComplex}{dt} = \gamma_2 \cdot [gRNA] \cdot [dCAS9] - \omega \cdot [Complex] \cdot P_y$$

$$\frac{dP_y^-}{dt} = \omega \cdot [Complex] \cdot P_y$$

$$\frac{dM}{dt} = \alpha_m \cdot P_Y - \delta_m \cdot [M] - K_i \cdot [M] + K_e \cdot [M_i]$$

$$\frac{dM_i}{dt} = K_i \cdot [M] - K_e \cdot [M_i]$$

$$\frac{dG}{dt} = K_e \cdot [M_i] - \alpha_{gm} \cdot [G]$$

$$\frac{dG_m}{dt} = \alpha_{gm} \cdot [G]$$

$$P_y = P_y^{tot} - P_y^- \quad (2)$$

2.3. STAR Models

STAR activates transcription by interacting with the target template to permit downstream gene expression. The original STAR model was adopted from a previous STAR modeling framework [39] and contains five dynamic states, STAR RNA, target mRNA, an intermediate RNA, immature GFP, and mature GFP, and the model has eight fitted kinetic parameters as in Equation (3). Where, P_S and P_Y are the fixed STAR and target template concentrations. The parameter α_S is the transcription rate of STAR RNA, and δ_S is the STAR RNA degradation rate. The parameter β_S describes STAR dependent hybridization or activation of the target template. The parameter α_m is the transcription rate of target mRNA following STAR activation, whereas δ_m is the target mRNA degradation rate. K_i and K_e describe the effective forward and reverse rates associated with the translation intermediate M_i. Finally, α_{gm} is the GFP maturation rate that converts G to G_m.

$$\frac{dSTAR}{dt} = \alpha_S \cdot P_S - \delta_S \cdot [STAR] - \beta_S \cdot P_Y \cdot [STAR]$$

$$\frac{dM}{dt} = \alpha_m \cdot \beta_S \cdot P_Y \cdot [STAR] - \delta_m \cdot [M] - K_i \cdot [M] + K_e \cdot [M_i]$$

$$\frac{dM_i}{dt} = K_i \cdot [M] - K_e \cdot [M_i]$$

$$\frac{dG}{dt} = K_e \cdot [M_i] - \alpha_{gm} \cdot [G]$$

$$\frac{dG_m}{dt} = \alpha_{gm} \cdot [G] \quad (3)$$

A reduced STAR model was then constructed to determine whether a lower-dimensional representation could render the model parameters structurally identifiable from GFP measurements. Rather than explicitly representing each intermediate molecular process, the reduced model retains only the effective long-timescale dynamics reflected in the fluorescence output: an effective STAR-mediated expression state, an activated GFP-production state, and mature GFP. The resulting model consists of three state variables and four parameters: an effective transcriptional rate (α), a STAR–target binding rate (β_S), an RNA degradation rate (δ), and a GFP degradation rate (δ_G), as defined in Equation (4).

$$\frac{dSTAR}{dt} = \alpha \cdot P_S - \delta \cdot [STAR] - \beta_S \cdot P_Y \cdot [STAR]$$

$$\frac{dM}{dt} = \alpha \cdot \beta_S \cdot P_Y \cdot [STAR] - \delta \cdot [M]$$

$$\frac{dG_m}{dt} = \alpha \cdot [M] - \delta_G \cdot [G_m] \quad (4)$$

A complete list of the state variables and kinetic parameters for the AND-gate, CRISPRi, and STAR (original and reduced) models, with their descriptions and units, is provided in the Supplementary Material (Tables S1–S4).

2.4. Objective Functions

For all models, the associated kinetic parameters were estimated by fitting the model predicted GFP output to the corresponding GFP fluorescence measurements. Let y_i denote the mean measured GFP value at time point i, let $\hat{y}_i(\theta)$ denote the model prediction for parameter vector θ, and let s_i^2 denote the sample variance estimated from the replicate measurements at time point i. Three objective functions were evaluated in order to compare parameterization without variance weighting, with inverse-variance weighting, and with relative-variance weighting. This comparison was motivated by the general finding that parameter estimation in mechanistic models depends not only on the model structure and the experimental data, but also on the assumed connection between simulations and noisy measurements [24,40]. The baseline objective is the unweighted sum of squared errors:

$$J_{SSE}(\boldsymbol{\theta}) = \sum_{i=1}^{n} (\hat{y}_i(\boldsymbol{\theta}) - y_i)^2 \quad (5)$$

The inverse-variance-weighted objective is defined as:

$$J_{Var}(\boldsymbol{\theta}) = \sum_{i=1}^{n} \frac{(\hat{y}_i(\boldsymbol{\theta}) - y_i)^2}{s_i^2} \quad (6)$$

which increases the influence of time points with smaller estimated variance. The relative-variance-weighted objective is defined as:

$$J_{RV}(\boldsymbol{\theta}) = \sum_{i=1}^{n} \frac{y_i^2}{s_i^2} (\hat{y}_i(\boldsymbol{\theta}) - y_i)^2 \tag{7}$$

In the relative-variance objective, the normalized variance was used, with y_i bounded to be at least 10^{-6}, and any variance below 10^{-6} was set to 10^{-6}. Because the measured GFP concentration starts from zero, the summation began at the first nonzero time point to avoid invalid division.

2.5. Toehold-Switch AND Gate and CRISPRi Data Noise Augmentation

To examine robustness as the measurement uncertainty increased, the AND-gate and CRISPRi datasets were analyzed under three data conditions: the raw experimental data, and data augmented with 20% and 40% signal proportional noise added to the mean of each raw data point. The two levels were selected relative to the variability of our cell-free measurements, in which the relative spread of the GFP signal across three replicates is typically about 10%. The 20% and 40% levels therefore correspond to approximately twice and four times this baseline variability, allowing us to test the parameterization as the measurement uncertainty is increased beyond the level normally observed. For each time point i and a replicate k, the augmented value was generated as:

$$y_{i,k}^{art} = \max(0, y_i + \eta_{i,k}), \qquad \eta_{i,k} \sim N(0, (\rho y_i)^2) \tag{8}$$

with $\rho = 0.20$ and $\rho = 0.40$ for the two noise levels. Six artificial replicate trajectories were generated for each condition, negative values were set to zero, and the time matched sample variances were computed from these replicates and used in the weighted objectives. This produced nine calibration scenarios per circuit for each tested objective function.

2.6. STAR Synthetic Data Generation

As a validation system, we collected two datasets from the STAR system: TXTL experimental measurements at a STAR plasmid concentration of 8 nM (*i.e.*, $P_s = 8$ nM) from [39], and a synthetic dataset generated based on these measurements. To construct the synthetic dataset, we first defined a reference set of "true" kinetic parameters for the STAR model. These reference parameters were obtained by fitting the model to the mean experimental expression trajectory using a genetic algorithm [41–43] with an unweighted pairwise mean squared error objective function, *i.e.*, $J = \sum_{i=1}^{K} (y_i^{simu} - y_i^{true})^2$, where y_i^{simu} and y_i^{true} are the simulated and experimentally measured GFP concentration at discrete time i. $K = 49$ corresponds to the 240 min of experimental duration. Note that this set of "True" kinetic parameters should not be confused with the biologically true kinetic parameters, as they would only capture the dynamics of the measured GFP data and are used to generate a controlled set of synthetic data for our analysis. The specific value of each parameter is given in Table 1. Using this reference parameter set, we simulated the STAR system under the $P_s = 8$ nM condition. We then applied the same noise-augmentation procedure to generate 100 synthetic datasets, each containing three replicate simulations to mimic standard experimental practice. This synthetic dataset provides a more controlled framework for evaluating the impact of measurement variance, complements the experimental measurements, and follows a common strategy used in biostatistical studies.

Table 1. Kinetic parameter information for STAR system synthetic data generation, true values are from the STAR experiment with $P_s = 8$ nM condition, parameters in all fittings are confined within the specified ranges.

Parameter	Description	True Value	Range for Fitting
α_s	STAR RNA transcription rate	2.198 s^{-1}	10^{-2}~10^{1} s^{-1}
δ_s	STAR RNA degradation rate	3.4843×10^{-4} s^{-1}	10^{-5}~10^{-1} s^{-1}
δ_m	EGFP mRNA degradation rate	0.279 s^{-1}	10^{-5}~10^{-1} s^{-1}

β_s	STAR binding rate	1.004×10^3 nM^{-1}	10^3~10^7 nM^{-1}
α_m	Lumped STAR activation and transcription rate	92.231 s^{-1}	10^{-2}~10^2 s^{-1}
K_i	EGFP translation initiation rate	0.001 s^{-1}	10^{-4}~10^{-2} s^{-1}
K_e	EGFP translation elongation rate	0.0025 s^{-1}	10^{-4}~10^{-2} s^{-1}
α_{gm}	EGFP maturation rate	0.011 s^{-1}	10^{-3}~10^{-1} s^{-1}

2.7. Parameter Optimization

Parameters were estimated using the MATLAB genetic algorithm, which is well suited for nonlinear objective functions with many parameters and potential local minima [41,44]. Each parameter was constrained to a biologically plausible range based on values reported in the literature [45–50]. For each AND-gate and CRISPRi scenario, 30 independent optimization runs were performed to characterize variability arising from the stochastic search and to reveal broad or boundary-concentrated parameter distributions that could be obscured by a single optimum. The genetic algorithm used a population size of 100, a maximum of 100 generations, and a function tolerance of 10^{-8}. The same settings were used when fitting the STAR models to the TXTL experimental measurements. However, for the 100 synthetic datasets, only one optimization run was performed per dataset for computational efficiency.

2.8. Identifiability Analysis

To analyze parameter identifiability, we adopted two complementary methods. Practical identifiability in the AND-gate and CRISPRi models was assessed using profile likelihood: one parameter was fixed over a prescribed range while the remaining parameters were re-optimized, and the increase in the profile objective relative to its minimum was used to classify each parameter as bounded, one-sided, weakly bounded, or practically non-identifiable, as illustrated in Figure 2 [30,40]. In Figure 2, ΔJ_{PL} denotes the increase in the profile objective relative to its minimum, $\Delta J_{PL} = J_{fixed} - J_{min}$. For a least-squares fit with approximately Gaussian error, the objective is proportional to the negative log-likelihood, so $2 \cdot \Delta J_{PL}$ is asymptotically χ^2-distributed with one degree of freedom. The 95% confidence threshold for a single parameter is therefore $\Delta J_{PL} = \chi^2(0.95,1)/2 = 3.84/2 = 1.92$, and a parameter is identifiable in a given direction when its profile exceeds this value on that side of the minimum [30]. This analysis quantifies how strongly the available GFP trajectories constrain each parameter, rather than establishing structural identifiability. Structural identifiability was then examined using GenSSI 2.0, a MATLAB R2022B toolbox that generates successive Lie derivatives and evaluates the rank of the resulting identifiability tableau [35,51]. GenSSI 2.0 was attempted for the AND-gate and CRISPRi models, but the required high-order symbolic Lie-derivative calculations were not computationally feasible in the available environment. This outcome does not classify either model as identifiable or non-identifiable; therefore, profile likelihood is reported as the identifiability analysis for these two complex circuits. For both STAR models, GenSSI 2.0 was applied with a fixed STAR input of 8 nM and a fixed target plasmid concentration of 0.5 nM, zero initial states, and GFP as the sole observable. Successive Lie derivatives were computed until the Jacobian rank stabilized [22,23,35,51].

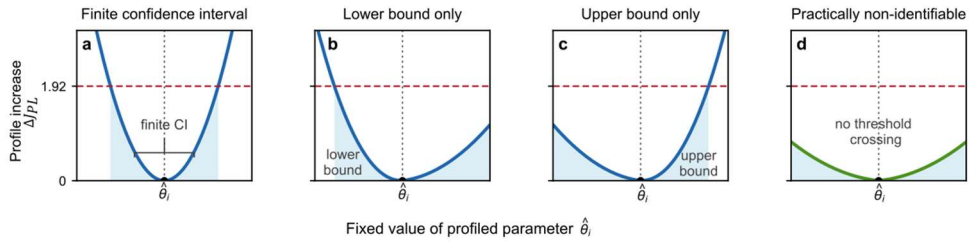


Figure 2. Conceptual interpretation of profile-likelihood behavior for parameter identifiability analysis. The quantity ΔJ_{PL} denotes the increase in the profile objective function relative to its minimum value, and the dashed line indicates the threshold

(1.92) corresponding to the 95% confidence interval. (**a**) Finite confidence interval, in which the profile exceeds the threshold on both sides of the minimum, yielding a bounded confidence interval. (**b**) Lower-bound case, in which the profile exceeds the threshold on only one side, yielding a lower bound on the parameter. (**c**) Upper-bound case, in which the profile exceeds the threshold on the opposite side, yielding an upper bound on the parameter. (**d**) Practically non-identifiable case, in which the profile does not exceed the threshold across the range considered.

3. Results

3.1. Objective Function Has a Minor Effect on Trajectory Fitting and Does Not Resolve Non-Identifiability in the AND-Gate and CRISPRi Models

We first examined two experimentally characterized circuits, the toehold-switch AND gate and the CRISPRi regulator, which represent cases in which the mechanistic models contain many unknown parameters while only GFP is experimentally observed. Both datasets exhibited replicate variability that changed over the course of the experiment, providing an appropriate setting to evaluate the three objective functions. We compared performance using the original experimental data and datasets augmented with 20% and 40% additional noise.

Across all nine scenarios, the three objective functions reproduced the measured GFP trajectories with similar accuracy, as shown for the AND gate in Figure 3a and the CRISPRi circuit in Figure 3b. The No Variance objective provided a reliable baseline. The Relative Variance objective showed greater robustness in several high-noise cases, particularly at later time points where signal-proportional variability was largest, because normalizing by signal magnitude reduces the disproportionate influence of high-magnitude measurements. In contrast, the Variance objective was the least consistent. When individual time points exhibited small empirical variances, those measurements received disproportionately large weights, causing the fitted trajectories to deviate from the overall experimental trend. This effect became less pronounced after additional noise was introduced, as the estimated variances increased and the heteroscedasticity became more evident.

Overall, however, the differences among the three objective functions were modest. Variance weighting altered the residual landscape and shifted the fitted trajectories and parameter estimates, but it did not produce a meaningfully better fit for these systems. These results indicate that unweighted least squares is already sufficient for accurate trajectory fitting in the tested AND-gate and CRISPRi models.

An accurate output fitting, however, does not establish that the underlying parameters are uniquely determined, and we therefore examined how strongly the data constrain each parameter. The most direct approach is structural identifiability analysis, which determines from the model equations whether the parameters can, in principle, be recovered from the chosen observable. We attempted this analysis using GenSSI 2.0, but for both the AND-gate and CRISPRi models, the symbolic Lie-derivative calculations did not converge. Because the models are large and highly coupled, the computation progressed to increasingly high derivative orders and ran for several days without reaching a stable rank in the available computational environment. This outcome does not classify the models as identifiable or non-identifiable; rather, it indicates that direct symbolic analysis is computationally intractable at this scale. We therefore turned to profile likelihood, which evaluates each parameter numerically by fixing it over a range of values and re-optimizing the remaining parameters, as a practical approach for assessing identifiability in these two complex circuit models.

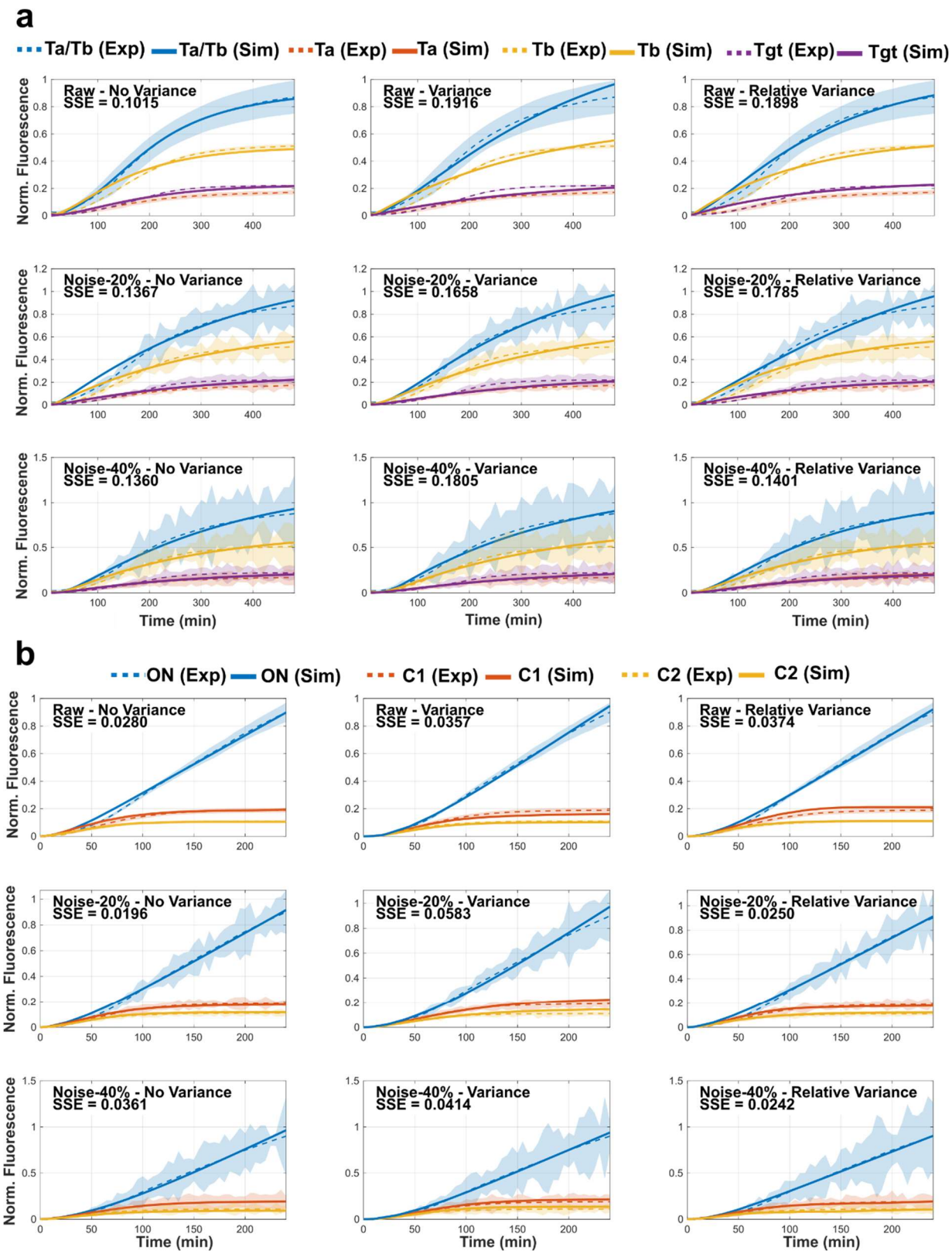


Figure 3. GFP trajectory fits for the toehold-switch AND gate (**a**) and the CRISPRi circuit (**b**) under the No Variance, Variance, and Relative Variance objectives, for raw experimental data and data augmented with 20% and 40% signal-proportional noise. The three objectives produced broadly comparable trajectories; Relative Variance was modestly more robust in selected high-noise cases, whereas raw Variance weighting was less consistent.

Profile likelihood analysis showed consistent behavior across the tested scenarios. Repeated optimization shifted several fitted parameter distributions as the objective function changed, but the

representative profiles remained shallow, one-sided, or bounded on only one side in most cases, while additional noise further broadened the profiles (Figure 4 for the AND gate and Figure 5 for CRISPRi). Note that the local fluctuations and multiple minima observed in these profiles arise from challenges in numerically solving the optimization problem due to the nonlinearity of the objective function, rather than from the underlying profile likelihood itself. As a result, these fluctuations primarily reflect optimization difficulties and do not, by themselves, provide direct evidence regarding parameter identifiability. Thus, the choice of objective function changed where the optimizer converged along a weakly constrained parameter surface, but it did not transform poorly constrained parameters into well-determined ones. This behavior is consistent with the structure of the models: the AND-gate model contains approximately twenty coupled parameters across four input conditions, whereas the CRISPRi model contains thirteen parameters across three conditions, with all parameters inferred from a single fluorescence output. Consequently, many different parameter combinations can reproduce nearly identical trajectories [30,31]. The two complex circuits therefore support the same conclusions: the choice of objective function has only a minor effect on trajectory fitting and does not resolve the underlying parameter non-identifiability. These findings motivated a controlled study using a smaller circuit model, in which the source of non-identifiability could be examined more directly.

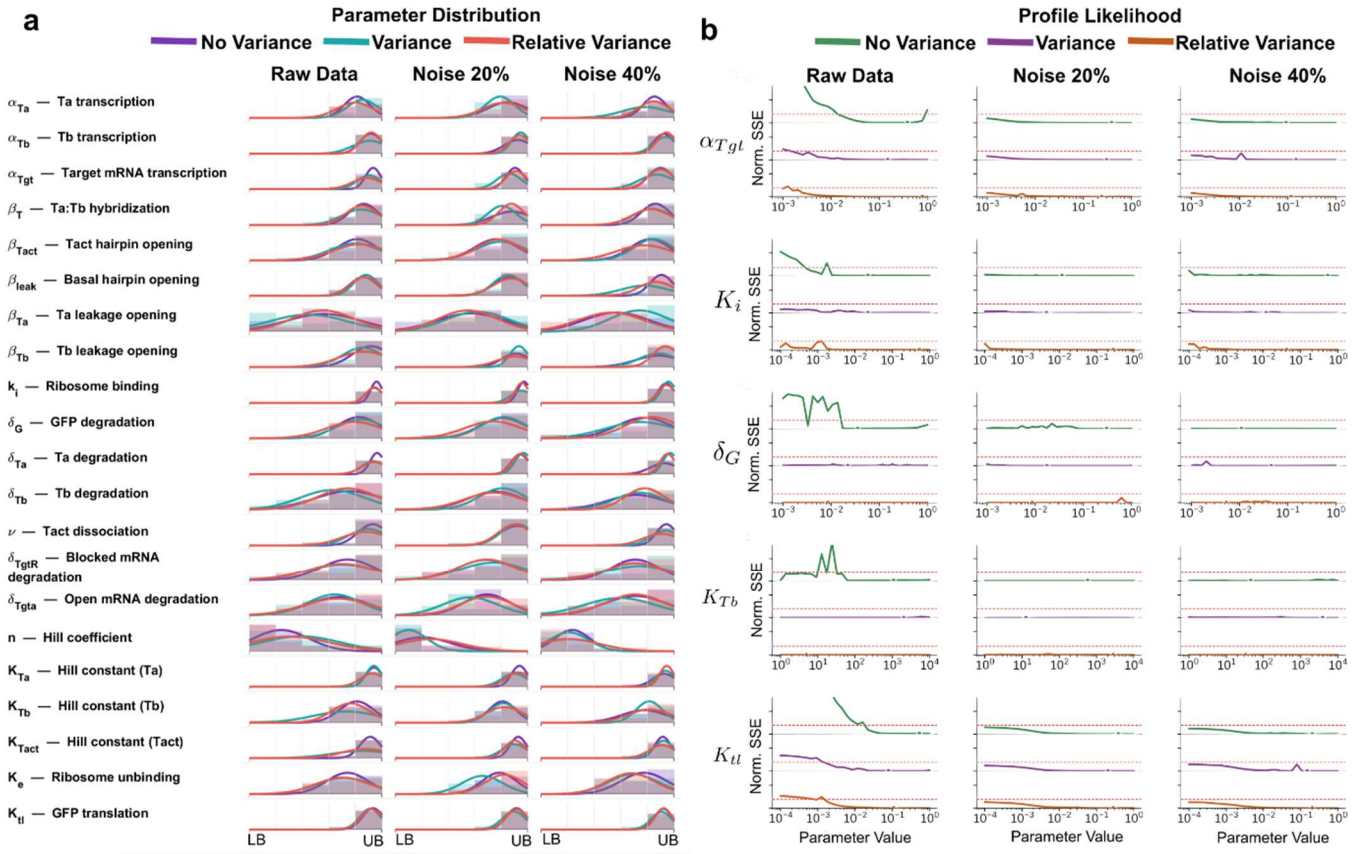


Figure 4. Fitted parameter distributions (**a**) and representative profile likelihoods (**b**) for the toehold-switch AND-gate model under raw, 20% noise, and 40% noise conditions using the three objectives. Objective-function choice shifted selected parameter distributions, but many profiles remained shallow, one-sided, irregular, or boundary-associated, indicating persistent practical non-identifiability that generally worsens as noise increases.

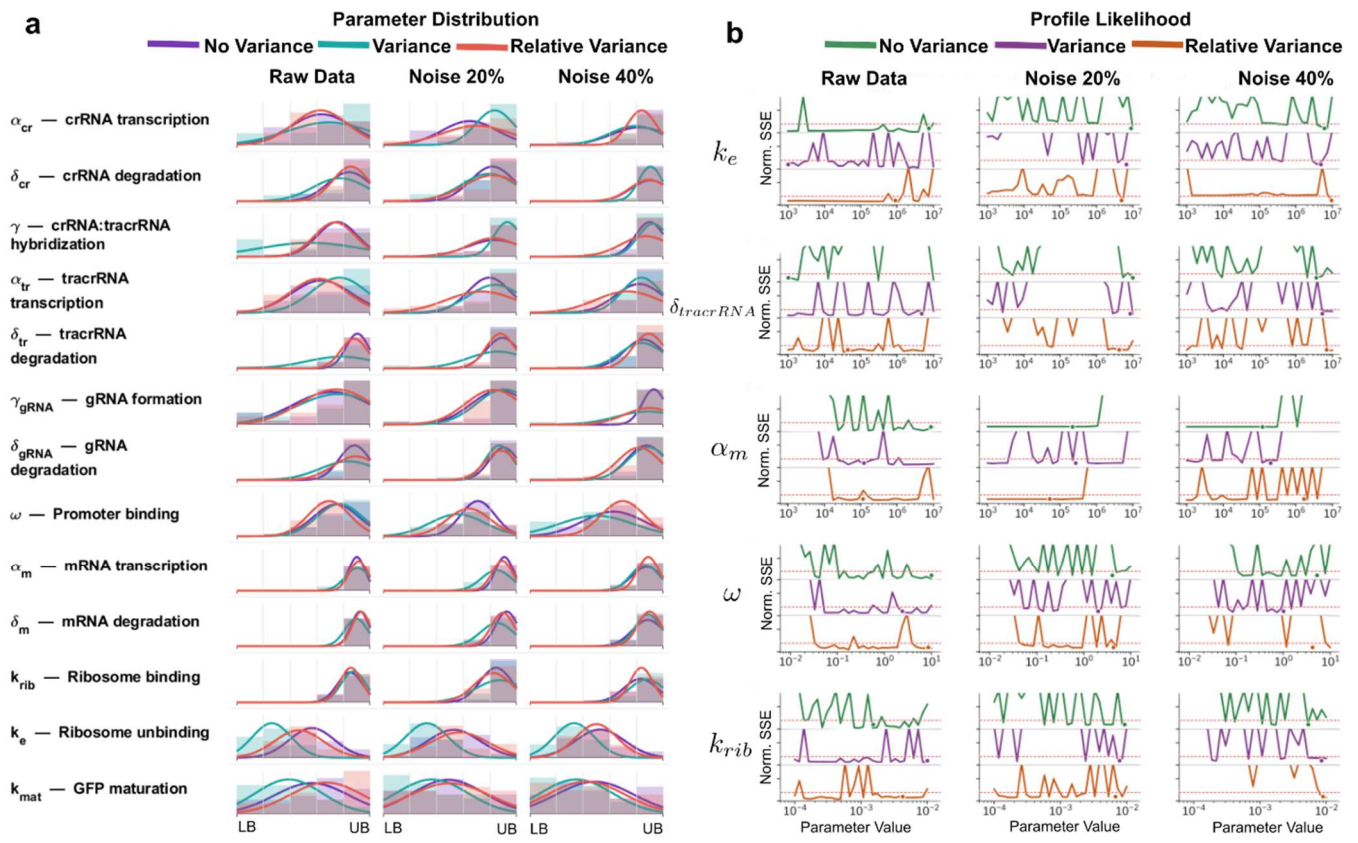


Figure 5. Fitted parameter distributions (**a**) and representative profile likelihoods (**b**) for the CRISPRi model under raw, 20% noise, and 40% noise conditions using the three objectives. Objective-function choice shifted selected parameter distributions, but many profiles remained shallow, one-sided, irregular, or boundary-associated, indicating persistent practical non-identifiability.

3.2. A Smaller Circuit Shows the Source of Non-Identifiability: The Original STAR Model Fits Well But Is Structurally Rank Deficient

To connect the numerical non-identifiability observed above to an exact structural cause, we analyzed the STAR system, whose smaller mechanistic model is amenable to symbolic analysis. We first fitted the original eight-parameter STAR model to 100 synthetic datasets generated from a reference parameter set using the three objective functions. The reference parameter set was obtained by fitting the model to the experimental 8 nM mean trajectory, so it serves as a controlled computational generator rather than a claim about the true biological rates.

As in the more complex circuits, the model reproduced the data while the parameters remained undetermined. Under all three objective functions, the model closely reproduced the mean synthetic trajectory (Figure 6a), yet the fitted parameter distributions remained broad, with several rate parameters spanning orders of magnitude (Figure 6b–i). Accurate trajectory fitting therefore did not correlate with recovery of the underlying kinetic parameters, as shown in Figure 6 (horizontal dashed lines). Analysis with GenSSI 2.0 demonstrated that, with GFP as the only observable for parameterization, the Jacobian rank stabilized at 5, whereas the model contains 8 free parameters, indicating that the model is rank deficient by three dimensions. This further suggests that additional measurements or model reduction are needed if parameter identification is the ultimate goal.

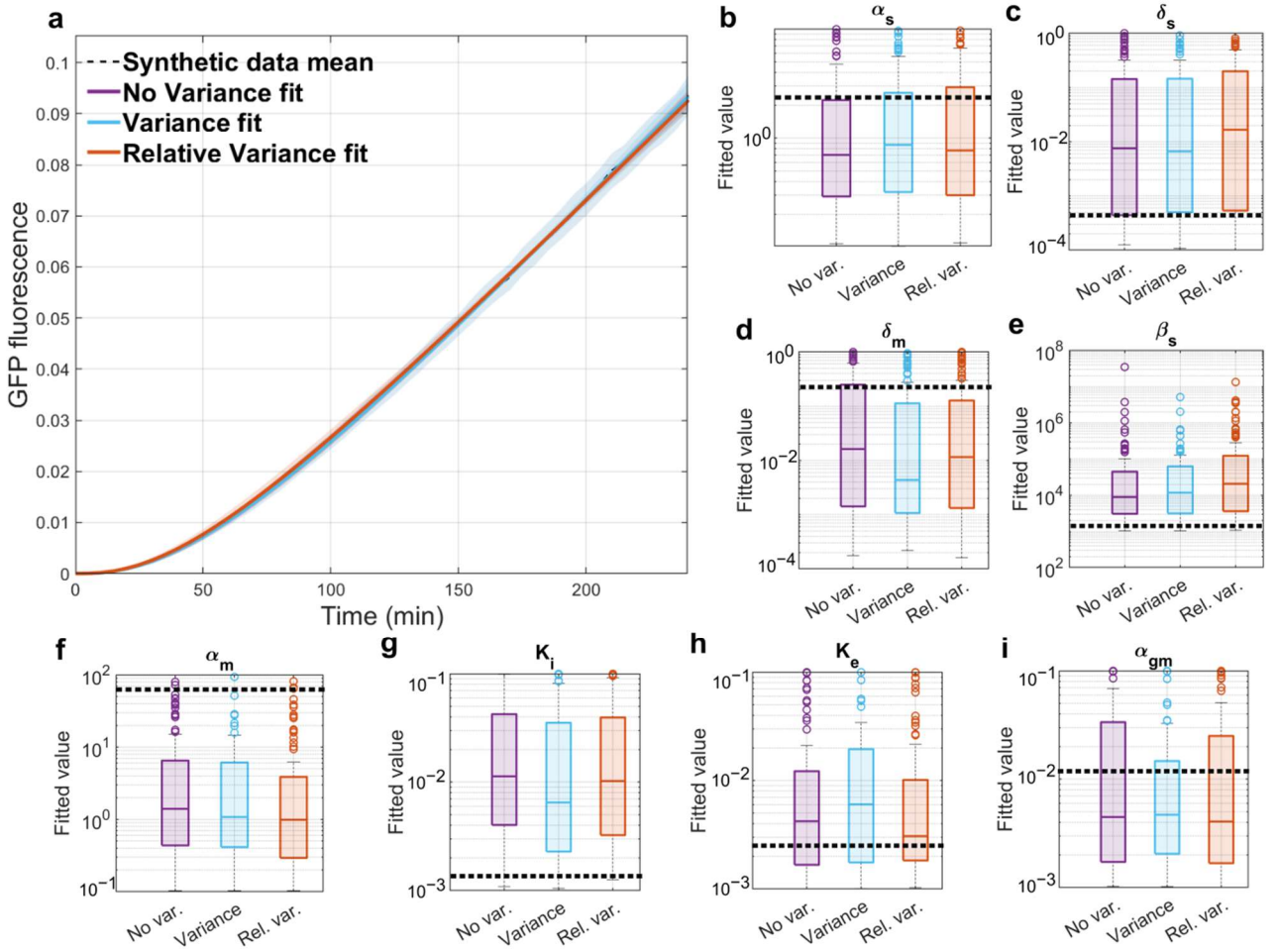


Figure 6. Original eight-parameter STAR model fitted to 100 synthetic heteroscedastic datasets. (**a**) Mean synthetic GFP trajectory (black dashed line) and fitted trajectories under the No Variance, Variance, and Relative Variance objectives; shaded bands show the spread across datasets. (**b**–**i**) Fitted distributions of the eight kinetic parameters across the 100 datasets. The dashed black lines represent the true parameters' values. Close output trajectories coexist with broad fitted parameter distributions.

3.3. Reduced Model Complexity Improves Structural Identifiability at the Cost of Fitting Fidelity

To test this hypothesis, we repeated the study using the reduced STAR model, which contains only three states and four parameters, as described in Section 2.3. Analysis with GenSSI 2.0 showed that the Jacobian matrix reached full rank of 4 for the four unknown parameters, first attaining full rank at Lie-derivative order 6, and classified the model as locally structurally identifiable. However, this improved identifiability was achieved at the cost of fitting accuracy, as demonstrated by the pronounced discrepancy between the fitted and reference data (synthetic data mean) in Figure 7. Specifically, the reduced model retained the overall growth pattern but deviated from the synthetic mean at both early and late times (Figure 7a), resulting in larger residual errors than the original model. The fitting also remained affected by noise, parameter scaling, objective-function choice, and model mismatch, as indicated by the parameter distributions in Figure 7b–e.

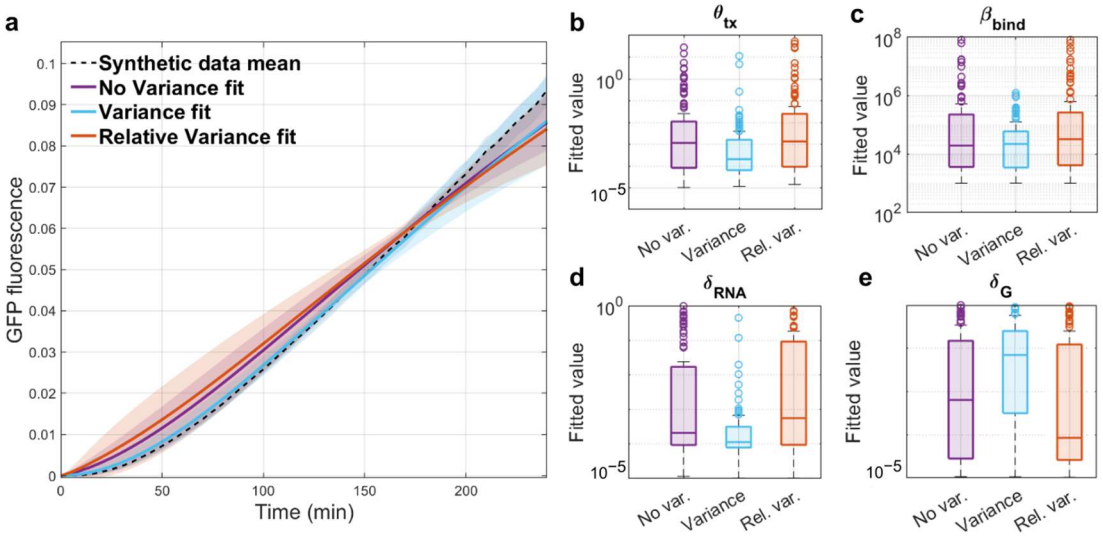


Figure 7. Reduced three-state, four-parameter STAR model fitted to 100 synthetic datasets. (**a**) Fitted trajectories under the No Variance, Variance, and Relative Variance objectives compared with the synthetic mean (black dashed line). (**b**–**e**) Fitted distributions of the four effective parameters. The reduced model is locally structurally identifiable by GenSSI 2.0, but fitting data generated by the richer original mechanism reveals the trajectory-fidelity cost of course-graining.

4. Discussions and Conclusions

In this work, we investigated a recurring question in gene circuit model calibration: whether measurement variance should be incorporated into the objective function for model parameterization. Using three RNA-based gene circuits, we further examined how objective-function formulation affects trajectory fitting and parameter identifiability.

Overall, the results suggest that unweighted least squares provide a dependable baseline for gene circuit parameterization. It accurately reproduced the AND-gate, CRISPRi, and STAR trajectories and was generally comparable to the weighted alternatives. Variance-aware weighting may be useful when measurement variability changes appreciably with time or signal magnitude; however, weighting based on relative variance produced more robust performance than direct inverse-variance weighting [24–26,28–30,52]. In the systems examined here, explicitly incorporating measurement variance did not consistently improve fitting performance.

The results also demonstrate that fitting performance and parameter identifiability are distinct properties. None of the tested objective functions resolved the non-identifiability observed in the more complex models, because residual weighting changes how a fixed dataset contributes to parameter estimation but does not increase the information contained in the measurements about the underlying kinetic parameters. When experimental information is limited, reducing model complexity can potentially improve local parameter identifiability, as demonstrated with the reduced STAR model, but this improvement may come at the cost of reduced fitting fidelity. Thus, achieving both detailed dynamic representation and identifiable parameter estimates will likely require more informative experiments, such as measurements of additional molecular species or targeted perturbations that isolate specific reactions, rather than changes in residual-weighting strategy alone [22,23,30,51]. Alternatively, increasing the measurable species can also improve the identifiability of model parameters. For example, in the current study, GFP is the only measured output used to infer the process dynamics, measuring associated RNA profiles alongside GFP could provide direct information on the transcription and RNA-processing rates, improving the identifiability of the related kinetic parameters [22,23].

Several limitations of this study should be noted. First, the synthetic noise was Gaussian and proportional to the signal and therefore does not capture all sources of variability in cell-free experiments,

such as batch-to-batch differences or baseline drift. In addition, variability introduced by the genetic-algorithm optimizer may contribute to the observed spread in fitted parameter values. Second, the GenSSI-based identifiability analyses were specific to the tested GFP-only measurement setting, and symbolic analysis was computationally tractable only for the smaller STAR models, but not for the larger AND-gate and CRISPRi models. Third, a parameter set fitted to a single experimental condition may not generalize to other conditions. Evaluating fitted models across multiple experimental conditions, rather than relying solely on calibration residuals from one condition, therefore provides a more reliable assessment of predictive validity. We also note that, in this study, we specifically focus on isolating the effects of measurement noise on deterministic model parameterization, and we assume that measurement noise follows a Gaussian distribution, consistent with common practice in previous studies [25,30,52]. While this assumption provides a reasonable approximation of measurement uncertainty under relevant experimental conditions, actual measurement noise may exhibit non-Gaussian distributions and signal-dependent variability. Furthermore, process-level stochasticity, arising from random biochemical reaction events such as transcriptional bursting, can produce non-Gaussian and temporally correlated fluctuations that may provide additional information for kinetic parameter identification. Model parameterization in such scenarios may require stochastic inference frameworks that account for the underlying distributional and temporal characteristics of biological dynamics [50,51], which the variance-weighting strategies investigated in this study may not adequately capture. Therefore, extending the findings of this study to systems exhibiting substantial process-level stochasticity would require further investigation and validation. Similarly, in vivo systems involve additional coupled processes, such as growth-related dilution and the allocation of ribosomes and other shared cellular resources [53]. These dynamics are inherent to the underlying biological dynamics rather than additive measurement noise in reporter signals. Therefore, directly extending the present analysis to in vivo systems may require modifications to the mechanistic models and, possibly, the objective functions to account for these additional dynamics. However, the general methodology presented in this study, including the introduction of synthetic noise into measurements for systematic evaluation and the parameter identifiability analysis, should remain applicable to in vivo systems analysis.

Taken together, these findings indicate that an unweighted pairwise squared-error objective provides a practical and satisfactory choice for the gene circuit models examined here, while relative-variance weighting may offer advantages when measurement variability is substantial and strongly dependent on signal magnitude. More importantly, improving trajectory fitting alone should not be interpreted as improving parameter identifiability. Future work should therefore investigate additional noise structures, model-form uncertainty, Bayesian inference, alternative identifiability-analysis methods, and, more broadly, the interplay among experimental information content, model complexity, objective-function formulation, and predictive performance.

Supplementary Materials

The following supporting information can be found at: https://www.sciepublish.com/article/pii/1331, Tables S1–S4 list the state variables and kinetic parameters of each model used in this study, together with a brief description and units for each symbol. Table S1: State variables and kinetic parameters of the toehold-switch AND-gate model (Equation (1)); Table S2: State variables and kinetic parameters of the CRISPRi model (Equation (2)); Table S3: State variables and kinetic parameters of the original STAR model (Equation (3)); Table S4: State variables and kinetic parameters of the reduced STAR model (Equation (4)).

Statement of the Use of Generative AI and AI-Assisted Technologies in the Writing Process

During the preparation of this manuscript, the authors used ChatGPT for language editing and references finding. After using this tool/service, the authors reviewed and edited the content as needed and take full responsibility for the content of the published.

Author Contributions

T.R.S.: acquisition of data, analysis and interpretation of data, drafting and revising the article. K.M.: acquisition of data. W.T.: conception and design, acquisition of data, analysis and interpretation of data, drafting and revising the article. X.T.: conception and design, acquisition of data, analysis and interpretation of data, drafting and revising the article.

Ethics Statement

Not applicable.

Informed Consent Statement

Not applicable.

Data Availability Statement

All MATLAB scripts used for this study are available on GitHub at https://github.com/xtang38/Thales-et-al-Objective-Function-2025.git.

Funding

X.T. and T.R.S. are supported by NSF grant no. 2223720.

Declaration of Competing Interest

The authors have no relevant financial or non-financial interests to disclose and declare no competing interests.

References

1. Brophy JAN, Voigt CA. Principles of Genetic Circuit Design. *Nat. Methods* **2014**, *11*, 508–520. DOI:10.1038/nmeth.2926
2. Ideker T, Galitski T, Hood L. A New Approach to Decoding Life: Systems Biology. *Annu. Rev. Genomics Hum. Genet.* **2001**, *2*, 343–372. DOI:10.1146/annurev.genom.2.1.343
3. Kitada T, DiAndreth B, Teague B, Weiss R. Programming Gene and Engineered-Cell Therapies with Synthetic Biology. *Science* **2018**, *359*, eaad1067. DOI:10.1126/science.aad1067
4. Lü J, Wang P. *Modeling and Analysis of Bio-Molecular Networks*; Springer: Singapore, 2020; ISBN 9789811591440
5. Spartalis TR, Lizano A, Copeland CE, Kwon YC, Tang X. Current Application of Modeling and Cell-Free System for Synthetic Gene Circuit Design. *Synth. Biol. Eng.* **2024**, *2*, 10013. DOI:10.35534/sbe.2024.10013
6. Wang YXR, Li L, Li JJ, Huang H. Network Modeling in Biology: Statistical Methods for Gene and Brain Networks. *Statist. Sci.* **2021**, *36*, 89–108. DOI:10.1214/20-STS792
7. Barajas C, Del Vecchio D. Effects of Spatial Heterogeneity on Bacterial Genetic Circuits. *PLoS Comput. Biol.* **2020**, *16*, e1008159. DOI:10.1371/journal.pcbi.1008159
8. Barajas C, Del Vecchio D. Genetic Circuit-Host Ribosome Transactions: Diffusion-Reaction Model. In Proceedings of the 2019 American Control Conference (ACC), Philadelphia, PA, USA, 10–12 July 2019. DOI:10.23919/ACC.2019.8815240
9. Chu BK, Tse MJ, Sato RR, Read EL. Markov State Models of Gene Regulatory Networks. *BMC Syst. Biol.* **2017**, *11*, 14. DOI:10.1186/s12918-017-0394-4
10. Endler L, Rodriguez N, Juty N, Chelliah V, Laibe C, Li C, et al. Designing and Encoding Models for Synthetic Biology. *J. R. Soc. Interface* **2009**, *6*, S405–S417. DOI:10.1098/rsif.2009.0035.focus

11. Hu CY, Varner JD, Lucks JB. Generating Effective Models and Parameters for RNA Genetic Circuits. *ACS Synth. Biol.* **2015**, *4*, 914–926. DOI:10.1021/acssynbio.5b00077
12. McAdams HH, Shapiro L. Circuit Simulation of Genetic Networks. *Science* **1995**, *269*, 650–656. DOI:10.1126/science.7624793
13. Ogorelova D, Sadyrbaev F. Remarks on the Mathematical Modeling of Gene and Neuronal Networks by Ordinary Differential Equations. *Axioms* **2024**, *13*, 61. DOI:10.3390/axioms13010061
14. Stone A, Ryan J, Tang X, Tian XJ. Negatively Competitive Incoherent Feedforward Loops Mitigate Winner-Take-All Resource Competition. *ACS Synth. Biol.* **2022**, *11*, 3986–3995. DOI:10.1021/acssynbio.2c00318
15. Adhikari A, Vilkhovoy M, Vadhin S, Lim HE, Varner JD. Effective Biophysical Modeling of Cell Free Transcription and Translation Processes. *Front. Bioeng. Biotechnol.* **2020**, *8*, 539081. DOI:10.3389/fbioe.2020.539081
16. Dattner I, Gugushvili S, Laskorunskyi O. Model Selection for Ordinary Differential Equations: A Statistical Testing Approach. *Biom. J.* **2024**, *66*, e70013. DOI:10.1002/bimj.70013
17. Daun S, Rubin J, Vodovotz Y, Clermont G. Equation-Based Models of Dynamic Biological Systems. *J. Crit. Care* **2008**, *23*, 585–594. DOI:10.1016/j.jcrc.2008.02.003
18. Hasdemir D, Hoefsloot HCJ, Smilde AK. Validation and Selection of ODE Based Systems Biology Models: How to Arrive at More Reliable Decisions. *BMC Syst. Biol.* **2015**, *9*, 32. DOI:10.1186/s12918-015-0180-0
19. Selvaggio G, Cristellon S, Marchetti L. A Novel Hybrid Logic-ODE Modeling Approach to Overcome Knowledge Gaps. *Front. Mol. Biosci.* **2021**, *8*, 760077. DOI:10.3389/fmolb.2021.760077
20. Linden NJ, Kramer B, Rangamani P. Bayesian Parameter Estimation for Dynamical Models in Systems Biology. *PLoS Comput. Biol.* **2022**, *18*, e1010651. DOI:10.1371/journal.pcbi.1010651
21. Mitra ED, Hlavacek WS. Parameter Estimation and Uncertainty Quantification for Systems Biology Models. *Curr. Opin. Syst. Biol.* **2019**, *18*, 9–18. DOI:10.1016/j.coisb.2019.10.006
22. Villaverde AF, Barreiro A, Papachristodoulou A. Structural Identifiability of Dynamic Systems Biology Models. *PLoS Comput. Biol.* **2016**, *12*, e1005153. DOI:10.1371/journal.pcbi.1005153
23. Wieland FG, Hauber AL, Rosenblatt M, Tönsing C, Timmer J. On Structural and Practical Identifiability. *Curr. Opin. Syst. Biol.* **2021**, *25*, 60–69. DOI:10.1016/j.coisb.2021.03.005
24. Ashyraliyev M, Fomekong-Nanfack Y, Kaandorp JA, Blom JG. Systems Biology: Parameter Estimation for Biochemical Models. *FEBS J.* **2009**, *276*, 886–902. DOI:10.1111/j.1742-4658.2008.06844.x
25. Murphy RJ, Maclaren OJ, Simpson MJ. Implementing Measurement Error Models with Mechanistic Mathematical Models in a Likelihood-Based Framework for Estimation, Identifiability Analysis and Prediction in the Life Sciences. *J. R. Soc. Interface* **2024**, *21*, 20230402. DOI:10.1098/rsif.2023.0402
26. Raue A, Schilling M, Bachmann J, Matteson A, Schelke M, Kaschek D, et al. Lessons Learned from Quantitative Dynamical Modeling in Systems Biology. *PLoS ONE* **2013**, *8*, e74335. DOI:10.1371/journal.pone.0074335
27. Tellinghuisen J. Weighted Least-Squares in Calibration: What Difference Does It Make? *Analyst* **2007**, *132*, 536–543. DOI:10.1039/b701696d
28. Brun R, Reichert P, Künsch HR. Practical Identifiability Analysis of Large Environmental Simulation Models. *Water Resour. Res.* **2001**, *37*, 1015–1030. DOI:10.1029/2000WR900350
29. Franceschini G, Macchietto S. Model-Based Design of Experiments for Parameter Precision: State of the Art. *Chem. Eng. Sci.* **2008**, *63*, 4846–4872. DOI:10.1016/j.ces.2007.11.034
30. Raue A, Kreutz C, Maiwald T, Bachmann J, Schilling M, Klingmüller U, et al. Structural and Practical Identifiability Analysis of Partially Observed Dynamical Models by Exploiting the Profile Likelihood. *Bioinformatics* **2009**, *25*, 1923–1929. DOI:10.1093/bioinformatics/btp358
31. Lillacci G, Khammash M. Parameter Estimation and Model Selection in Computational Biology. *PLoS Comput. Biol.* **2010**, *6*, e1000696. DOI:10.1371/journal.pcbi.1000696
32. Green AA, Silver PA, Collins JJ, Yin P. Toehold Switches: De-Novo-Designed Regulators of Gene Expression. *Cell* **2014**, *159*, 925–939. DOI:10.1016/j.cell.2014.10.002
33. Larson MH, Gilbert LA, Wang X, Lim WA, Weissman JS, Qi LS. CRISPR Interference (CRISPRi) for Sequence-Specific Control of Gene Expression. *Nat. Protoc.* **2013**, *8*, 2180–2196. DOI:10.1038/nprot.2013.132
34. Tickman BI, Burbano DA, Chavali VP, Kiattisewee C, Fontana J, Khakimzhan A, et al. Multi-Layer CRISPRa/i Circuits for Dynamic Genetic Programs in Cell-Free and Bacterial Systems. *Cell Syst.* **2022**, *13*, 215–229.e8. DOI:10.1016/j.cels.2021.10.008
35. Green AA, Kim J, Ma D, Silver PA, Collins JJ, Yin P. Complex Cellular Logic Computation Using Ribocomputing Devices. *Nature* **2017**, *548*, 117–121. DOI:10.1038/nature23271

36. Kim J, Zhou Y, Carlson PD, Teichmann M, Chaudhary S, Simmel FC, et al. De Novo-Designed Translation-Repressing Riboregulators for Multi-Input Cellular Logic. *Nat. Chem. Biol.* **2019**, *15*, 1173–1182. DOI:10.1038/s41589-019-0388-1
37. Spartalis TR, Porche KB, Tang X, Kwon YC. Cell-Free Genetic Circuits: Extract and Template Preparation. In *Synthetic Gene Circuits*; Tian XJ, Ed.; Springer: New York, NY, USA, 2026. DOI:10.1007/978-1-0716-5304-3_9
38. Westbrook A, Tang X, Marshall R, Maxwell CS, Chappell J, Agrawal DK, et al. Distinct Timescales of RNA Regulators Enable the Construction of a Genetic Pulse Generator. *Biotechnol. Bioeng.* **2019**, *116*, 1139–1151. DOI:10.1002/bit.26918
39. Simpson MJ, Maclaren OJ. Profile-Wise Analysis: A Profile Likelihood-Based Workflow for Identifiability Analysis, Estimation, and Prediction with Mechanistic Mathematical Models. *PLoS Comput. Biol.* **2023**, *19*, e1011515. DOI:10.1371/journal.pcbi.1011515
40. Daly AC, Gavaghan D, Cooper J, Tavener S. Inference-Based Assessment of Parameter Identifiability in Nonlinear Biological Models. *J. R. Soc. Interface* **2018**, *15*, 20180318. DOI:10.1098/rsif.2018.0318
41. Holland JH. Genetic Algorithms. *Sci. Am.* **1992**, *267*, 66–72. DOI:10.1038/scientificamerican0792-66
42. Balleza E, Kim JM, Cluzel P. Systematic Characterization of Maturation Time of Fluorescent Proteins in Living Cells. *Nat. Methods* **2018**, *15*, 47–51. DOI:10.1038/nmeth.4509
43. Liu H, Hong F, Smith F, Goertz J, Ouldridge T, Stevens MM, et al. Kinetics of RNA and RNA:DNA Hybrid Strand Displacement. *ACS Synth. Biol.* **2021**, *10*, 3066–3073. DOI:10.1021/acssynbio.1c00336
44. Marshall R, Noireaux V. Quantitative Modeling of Transcription and Translation of an All-*E. coli* Cell-Free System. *Sci. Rep.* **2019**, *9*, 11980. DOI:10.1038/s41598-019-48468-8
45. Ryan J, Hong S, Foo M, Kim J, Tang X. Model-Based Investigation of the Relationship between Regulation Level and Pulse Property of I1-FFL Gene Circuits. *ACS Synth. Biol.* **2022**, *11*, 2417–2428. DOI:10.1021/acssynbio.2c00109
46. Shin J, Noireaux V. Study of Messenger RNA Inactivation and Protein Degradation in an *Escherichia coli* Cell-Free Expression System. *J. Biol. Eng.* **2010**, *4*, 9. DOI:10.1186/1754-1611-4-9
47. Todisco M, Szostak JW. Hybridization Kinetics of Out-of-Equilibrium Mixtures of Short RNA Oligonucleotides. *Nucleic Acids Res.* **2022**, *50*, 9647–9662. DOI:10.1093/nar/gkac784
48. Chis OT, Banga JR, Balsa-Canto E. Structural Identifiability of Systems Biology Models: A Critical Comparison of Methods. *PLoS ONE* **2011**, *6*, e27755. DOI:10.1371/journal.pone.0027755
49. Spiegelman D, Logan R, Grove D. Regression Calibration with Heteroscedastic Error Variance. *Int. J. Biostat.* **2011**, *7*, 000010220215574679 1259. DOI:10.2202/1557-4679.1259
50. Schnoerr D, Sanguinetti G, Grima R. Approximation and Inference Methods for Stochastic Biochemical Kinetics—A Tutorial Review. *J. Phys. A Math. Theor.* **2017**, *50*, 093001. DOI:10.1088/1751-8121/aa54d9
51. Zechner C, Ruess J, Krenn P, Pelet S, Peter M, Lygeros J, et al. Moment-Based Inference Predicts Bimodality in Transient Gene Expression. *Proc. Natl. Acad. Sci. USA* **2012**, *109*, 8340–8345. DOI:10.1073/pnas.1200161109
52. Markakis K, De Las Heras A, Elfick A. Analytical Approach for the Calculation of Promoter Activities Based on Fluorescent Protein Expression Data. *Eng. Biol.* **2017**, *1*, 77–85. DOI:10.1049/enb.2017.0002
53. Gorochowski TE, Avcilar-Kucukgoze I, Bovenberg RAL, Roubos JA, Ignatova Z. A Minimal Model of Ribosome Allocation Dynamics Captures Trade-offs in Expression between Endogenous and Synthetic Genes. *ACS Synth. Biol.* **2016**, *5*, 710–720. DOI:10.1021/acssynbio.6b00040